Gauge-Protected $U(1)$ Quantum Links from Paired Square-Root Edge Ladders

Joshua Farrow[1]

[1] *Independent Research*

(Dated: June 20, 2026)

Finite-dimensional quantum links can realize an exact continuous gauge algebra while approaching Wilson lattice gauge theory in a controlled large-representation limit. We construct such a sector directly from two square-root ladder registers on every oriented edge, the local ingredient used by the QATNU substrate. Restricting their total occupation to $2S$ gives a Schwinger pair with electric field $E = (n_a - n_b)/2$ and link operator $U = a^\dagger b/\sqrt{S(S+1)}$. The transformation law $[E, U] = U$ is exact at every finite S, while the failure of link unitarity on a fixed low-flux window is bounded by $E_*(E_*+1)/[S(S+1)]$. Local Gauss generators, gauge-covariant charged-matter hopping, and plaquette loops follow exactly. A four-state mobile controller carrying one gauge charge generates the magnetic plaquette operator at fourth order without breaking the microscopic Gauss law. Number-sector and Gauss-law penalties suppress generic leakage with measured probabilities proportional to $\Delta_N^{-1.999}$ and $\Lambda^{-2.026}$, respectively. A low-flux single-plaquette spectrum converges to the rotor spectrum approximately as $S^{-1.915}$. In three spatial dimensions the resulting harmonic long-wavelength sector has two degenerate transverse branches, a lattice Ward residual below 3.7×10^{-15}, and an electrostatic Green function fitted by $A/r + B$ with $R^2 = 0.999926$ on a 128^3 lattice. The result is a constructive, gauge-protected $U(1)$/Maxwell sector in an explicit paired-ladder extension. It does not show that the original one-ladder QATNU Hamiltonian inevitably generates electromagnetism, nor does it prove the full nonperturbative Coulomb phase at fixed small S.

I. INTRODUCTION

Hamiltonian lattice gauge theory represents electric flux on oriented links and builds magnetic dynamics from gauge-invariant plaquette loops [1–3]. In Wilson's formulation the link variable is unitary and has an infinite-dimensional local Hilbert space. Quantum link models replace it by a finite matrix while retaining an exact continuous local gauge transformation law [4–6]. They provide both a finite-resource representation for quantum simulation [7–9] and a controlled route toward lattice QED as the link representation, volume, and spatial resolution are enlarged [10].

A separate line of work shows that local bosonic or spin systems can possess low-energy $U(1)$ Coulomb phases with linearly dispersing photons and Coulomb interactions [11, 12]. These results make an important distinction. One may *construct* a microscopic system whose selected low-energy sector is a gauge theory without proving that every superficially similar microscopic system flows to that sector.

This paper applies that distinction to the QATNU edge-register architecture. The only required microscopic ingredient is a finite square-root ladder,

$$r^\dagger|n\rangle = \sqrt{n+1}|n+1\rangle, \tag{1}$$

with a sufficiently high top rung. We add a second ladder to each oriented edge and select a fixed total occupation. The pair is then exactly a spin-S quantum link. This is an explicit local extension of the minimal one-ladder substrate; it is not a claim that the extension appears automatically.

The contributions are fivefold. First, we give the exact paired-ladder link algebra and a low-flux operator-norm bound for its approach to a unitary rotor link. Second, we construct the local Gauss law and gauge-covariant matter coupling. Third, a finite mobile controller generates the magnetic plaquette term through a gauge-invariant virtual loop. Fourth, link-number and Gauss penalties select and protect the target sector against generic microscopic perturbations. Fifth, the controlled large-S, low-flux, long-wavelength limit yields the harmonic Maxwell matrix, two transverse modes, and a three-dimensional Coulomb Green function.

The central status statement is therefore

> A paired square-root-ladder extension is sufficient to host an exact finite-dimensional $U(1)$ quantum-link theory whose controlled low-flux and long-wavelength sector is Maxwell-like.

It is deliberately not the stronger statement that the original unmodified QATNU Hamiltonian inevitably produces electromagnetism.

II. PAIRED LADDERS AS AN EXACT QUANTUM LINK

A. Fixed-number Schwinger sector

Assign two square-root ladders a_ℓ, b_ℓ to every oriented link $\ell = (x, y)$. Select

$$N_\ell = n_{a,\ell} + n_{b,\ell} = 2S, \qquad S \in \tfrac{1}{2}\mathbb{N}, \tag{2}$$

and define

$$E_\ell = \frac{n_{a,\ell} - n_{b,\ell}}{2}, \qquad U_\ell = \frac{a_\ell^\dagger b_\ell}{\sqrt{S(S+1)}}. \tag{3}$$

Both E_ℓ and U_ℓ commute with N_ℓ. The target link sector is therefore invariant exactly; an energy penalty is only

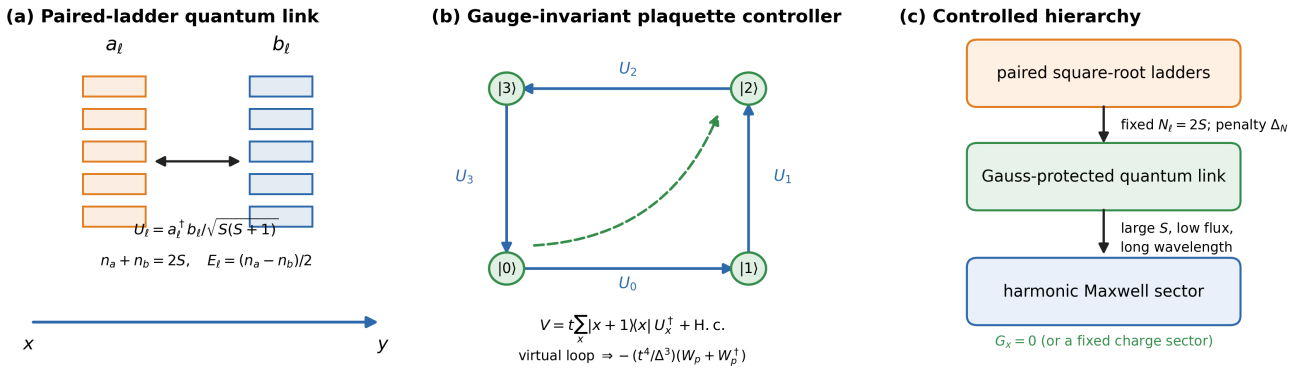

FIG. 1. Construction and scope. (a) Two square-root ladders at fixed total occupation give one finite $U(1)$ quantum link. (b) A mobile gauge charge generates the plaquette loop through local gauge-invariant virtual hops. (c) Maxwell behavior follows only after the paired-link sector, Gauss law, large-S/low-flux limit, and long-wavelength expansion are imposed.

required to make it robust against additional number-changing microscopic terms.

Proposition 1 (Exact finite-S link algebra)**.** *On the sector in Eq.* (2),

$$[E_\ell, U_\ell] = U_\ell, \qquad \mathrm{e}^{\mathrm{i}\alpha E_\ell} U_\ell \mathrm{e}^{-\mathrm{i}\alpha E_\ell} = \mathrm{e}^{\mathrm{i}\alpha} U_\ell, \tag{4}$$

and

$$U_\ell^\dagger U_\ell = \mathbb{I} - \frac{E_\ell(E_\ell+1)}{S(S+1)}, \tag{5}$$

$$U_\ell U_\ell^\dagger = \mathbb{I} - \frac{E_\ell(E_\ell-1)}{S(S+1)}. \tag{6}$$

The proof is the Schwinger representation $J^+ = a^\dagger b$, $J^z = E$. The gauge algebra is exact for every S; only the unitarity of the parallel transporter is approximate.

Let $\mathcal{P}_{E_*}$ project onto $|E_\ell| \le E_* < S$. Equations (5) and (6) imply

$$\epsilon_U(E_*) \equiv \max\Big\{\big\|\mathcal{P}_{E_*}(U^\dagger U - \mathbb{I})\mathcal{P}_{E_*}\big\|, \big\|\mathcal{P}_{E_*}(UU^\dagger - \mathbb{I})\mathcal{P}_{E_*}\big\|\Big\} \le \frac{E_*(E_*+1)}{S(S+1)}. \tag{7}$$

The commutator in Eq. (4) was verified through $S = 64$ with maximum elementwise error 4.22×10^{-15}. At fixed $E_* = 2$, the unitarity defect fits $S^{-1.930}$ over $S = 4$–64 and follows the exact $O(S^{-2})$ bound [Fig. 2(a)].

B. Controlled rotor limit

Let V denote the ideal bilateral shift on the electric-flux basis, $V|m\rangle = |m+1\rangle$. Away from the finite-S endpoints,

$$U|m\rangle = u_m|m+1\rangle, \qquad u_m = \sqrt{1 - \frac{m(m+1)}{S(S+1)}}. \tag{8}$$

For $|m| \le E_*$,

$$\|(U - V)\mathcal{P}_{E_*}\| \le \delta_S(E_*) \le \frac{E_*(E_*+1)}{S(S+1)}, \tag{9}$$

where $\delta_S = 1 - \sqrt{1 - E_*(E_*+1)/[S(S+1)]}$. A telescoping product then gives, for a four-link plaquette,

$$\left\|(W_p - W_p^{\mathrm{rotor}})\mathcal{P}_{E_*}^{(p)}\right\| \le 4\delta_S(E_*). \tag{10}$$

Thus, on any fixed low-flux window of a finite lattice, the quantum-link Hamiltonian converges in operator norm to the corresponding rotor Hamiltonian as S^{-2}.

As a spectral check, we diagonalized one charge-free plaquette. Gauss's law restricts it to equal electric flux on all four links, so W_p raises a common flux with amplitude u_m^4. The maximum error in the first five excitation gaps relative to an ideal rotor truncation scales as $S^{-1.915}$ for $S = 6$–64 [Fig. 2(b)]. This is a finite-volume diagnostic of the controlled link limit, not a proof of the thermodynamic Coulomb phase at small S.

III. LOCAL GAUGE STRUCTURE AND CHARGED MATTER

For an oriented spatial lattice, define

$$G_x = \sum_{\ell \text{ out of } x} E_\ell - \sum_{\ell \text{ into } x} E_\ell - Q_x. \tag{11}$$

Then

$$\mathrm{e}^{\mathrm{i}\sum_z \alpha_z G_z} U_{xy} \mathrm{e}^{-\mathrm{i}\sum_z \alpha_z G_z} = \mathrm{e}^{\mathrm{i}(\alpha_x - \alpha_y)} U_{xy}. \tag{12}$$

The physical sector is specified by $G_x|\psi\rangle = 0$ or by a chosen background-charge sector.

The oriented plaquette product

$$W_p = \prod_{\ell \in \partial p}^{\circlearrowleft} U_\ell \tag{13}$$

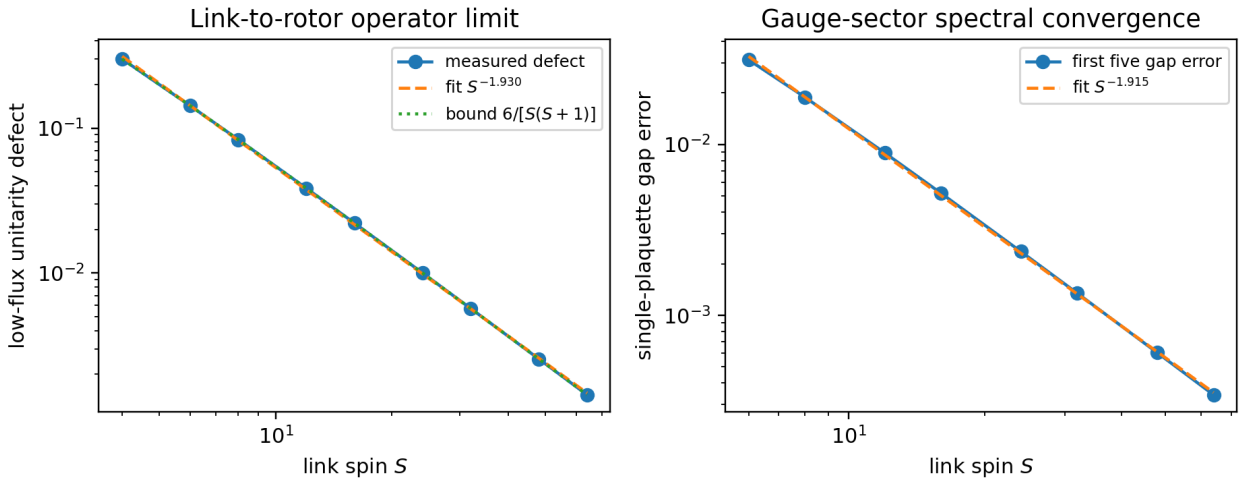

FIG. 2. Controlled large-S limit. (a) On $|E| \leq 2$, the finite-link unitarity defect follows the exact $6/[S(S+1)]$ bound. (b) In the charge-free one-plaquette sector, the first five quantum-link excitation gaps converge to the ideal rotor gaps with an approximately quadratic power.

commutes with every G_x. If c_x lowers a unit-charge matter occupation, the hopping term

$$H_{xy}^{\text{hop}} = t_m(c_x^\dagger U_{xy} c_y + \text{H.c.}) \tag{14}$$

also commutes with G_x and G_y. A one-link $S = 2$ matrix calculation gives both commutator norms exactly zero to machine precision.

The target Hamiltonian is

$$H_{\text{QL}} = \frac{g^2}{2a}\sum_\ell E_\ell^2 + \frac{1}{2g^2 a}\sum_p (2 - W_p - W_p^\dagger) + H_{\text{matter}} + \Delta_N \sum_\ell (N_\ell - 2S)^2 + \Lambda \sum_x G_x^2. \tag{15}$$

When restricted exactly to $N_\ell = 2S$ and $G_x = 0$, the final two terms vanish. At finite penalties they make the same target sector emerge as a separated low-energy manifold.

IV. A GAUGE-INVARIANT FINITE CONTROLLER FOR THE PLAQUETTE TERM

A four-link interaction need not be primitive. Place one mobile controller charge on the four vertices of a plaquette, with basis $|x\rangle$, $x = 0, 1, 2, 3$. Detune three positions,

$$H_0 = \Delta \sum_{x=1}^{3} |x\rangle\langle x|, \tag{16}$$

and let the charge hop clockwise while changing the traversed link flux,

$$V = t \sum_{x=0}^{3} \left(|x+1\rangle\langle x| \otimes U_x^\dagger + \text{H.c.} \right), \tag{17}$$

where controller labels are understood modulo four. The total Gauss generator is

$$\mathcal{G}_x = E_x - E_{x-1} - |x\rangle\langle x| + \delta_{x0}\mathbb{I}. \tag{18}$$

The last term is a static background charge that makes $|0\rangle$ with zero flux physical. Each microscopic hop in Eq. (17) satisfies

$$[\mathcal{G}_x, H_0 + V] = 0 \quad \forall x. \tag{19}$$

Thus gauge invariance is not restored only after the virtual process; it is exact at every intermediate step.

Let $P = |0\rangle\langle 0| \otimes \mathbb{I}$, $Q = \mathbb{I} - P$, and $R = -Q/\Delta$. The connected fourth-order operator is

$$PVRVRVRVP = -\frac{t^4}{\Delta^3}(W_p + W_p^\dagger) + H_{\text{diag}}^{(4)}, \tag{20}$$

where $H_{\text{diag}}^{(4)}$ contains backtracking counterterms. For $S = 1$, direct multiplication in the 324-dimensional controller-link Hilbert space gives an off-diagonal relative error 1.82×10^{-16}.

We also evaluated the exact zero-energy Schur complement rather than truncating at fourth order. The relative correction to the matrix element $-t^4/\Delta^3$ scales as $(t/\Delta)^{2.030}$ over the perturbative range [Fig. 3], as expected for the next even order. The construction is therefore both microscopically gauge invariant and quantitatively controlled by t/Δ.

V. SELECTING AND PROTECTING THE GAUGE SECTOR

The fixed-number and Gauss constraints are exact symmetries of the target Hamiltonian, but generic microscopic

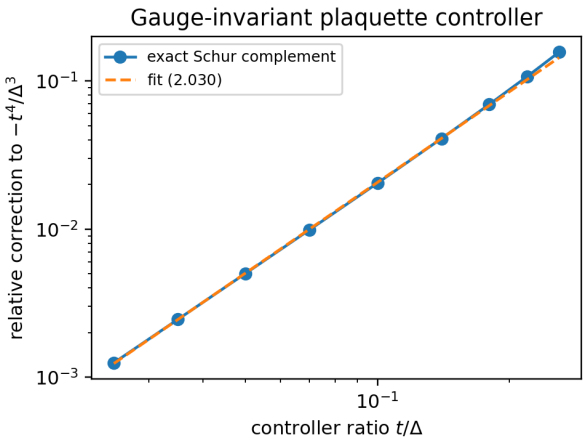

FIG. 3. Exact Schur-complement correction to the leading plaquette coupling generated by the gauge-invariant four-state controller. The relative error is quadratic in t/Δ, consistent with sixth-order corrections to a fourth-order ring term.

perturbations need not respect them. Both can be protected energetically.

For one paired link, add $\Delta_N(N-2S)^2$ and a bounded number-changing perturbation V_N. Starting in $N = 2S$, a direct $S = 2$ two-ladder evolution gives maximum leakage proportional to $\Delta_N^{-1.999}$ over the large-penalty range [Fig. 4(a)]. This establishes that the paired-link sector can be selected dynamically rather than imposed only as a kinematic deletion of states.

The Gauss law has the same structure. Let P project onto $G_x = 0$ for all x, $Q = \mathbb{I} - P$, and suppose

$$Q\sum_x G_x^2 Q \geq g_* Q, \qquad g_* > 0. \tag{21}$$

If $H_{\rm inv}$ commutes with every G_x and V_b is a bounded gauge-breaking perturbation, then any normalized eigenstate of

$$H_\Lambda = H_{\rm inv} + V_b + \Lambda \sum_x G_x^2 \tag{22}$$

with $|E| \leq E_*$ obeys

$$\|Q\psi\| \leq \frac{\|QV_bP\|}{\Lambda g_* - E_* - \|Q(H_{\rm inv}+V_b)Q\|}, \tag{23}$$

whenever the denominator is positive. Gauge-violation probability is therefore $O(\Lambda^{-2})$, consistent with established energy-protection analyses [13, 14].

On an $S = 1$ four-link plaquette with a generic single-link perturbation, the maximum leakage over $0 \leq t \leq 30$ scales as $\Lambda^{-2.026}$, while the leakage of the lowest gauge-sector-sized spectral subspace follows the same quadratic law [Fig. 4(b)]. The unperturbed Hamiltonian and the plaquette operator commute with all Gauss generators to machine precision.

VI. LONG-WAVELENGTH MAXWELL SECTOR

The exact finite-S algebra does not by itself imply a massless photon. The Maxwell sector arises after three controlled steps: restriction to low flux, large S so that U approaches a unitary shift, and a long-wavelength expansion of the deconfined rotor theory. This is the same hierarchy used in quantum-link and emergent-$U(1)$ constructions [6, 11, 12].

Write the low-flux link as

$$U_{x,i} = \mathrm{e}^{\mathrm{i}aA_i(x)} + O\!\left(\frac{E_*^2}{S^2}\right). \tag{24}$$

For a smooth field, the plaquette angle is $a^2F_{ij} + O(a^3\partial F)$, so

$$2 - W_p - W_p^\dagger = a^4 B_p^2 + O(a^6\partial^4 A^2) + O(E_*^2/S^2). \tag{25}$$

After the standard field rescaling, Eq. (15) becomes

$$H_{\rm Max} = \frac{1}{2}\int d^3x\, \left(g^2\boldsymbol{E}^2 + g^{-2}\boldsymbol{B}^2\right), \qquad \boldsymbol{\nabla}\cdot\boldsymbol{E} = \rho. \tag{26}$$

On a cubic lattice the magnetic matrix is

$$M_{ij}(\boldsymbol{k}) = \widetilde{k}^2\delta_{ij} - \widetilde{k}_i\widetilde{k}_j, \qquad \widetilde{k}_i = \frac{2}{a}\sin\frac{k_i a}{2}. \tag{27}$$

For every nonzero momentum it has eigenvalues $0, \widetilde{k}^2, \widetilde{k}^2$. Gauss's law removes the longitudinal zero branch, leaving

$$\omega_{1,2}(\boldsymbol{k}) = c\sqrt{\sum_i \widetilde{k}_i^2} \longrightarrow c|\boldsymbol{k}|. \tag{28}$$

The numerical Ward residual $\left\|M\widetilde{\boldsymbol{k}}\right\|$ is below 3.66×10^{-15} and the transverse splitting is below 3.55×10^{-15}. At $ka = 2\pi/128$, the lattice dispersion differs from $c|\boldsymbol{k}|$ by 1.00×10^{-4}.

The electrostatic response is the inverse lattice Laplacian with the periodic zero mode removed. On a 128^3 lattice, shell averaging over $4 \leq r \leq 20$ gives

$$G(r) = \frac{0.07810996}{r} - 0.00165925, \qquad R^2 = 0.999926. \tag{29}$$

The fitted coefficient is within 1.84% of $1/(4\pi) = 0.07957747$; the remaining difference is dominated by lattice and finite-volume corrections. Figure 5 displays both the transverse spectrum and Coulomb response.

VII. NUMERICAL IMPLEMENTATION AND AUDIT

All finite-link calculations were constructed directly in the electric-flux basis using dense or sparse matrix products. No gauge commutator was inferred from a fitted observable. Table I summarizes the load-bearing checks.

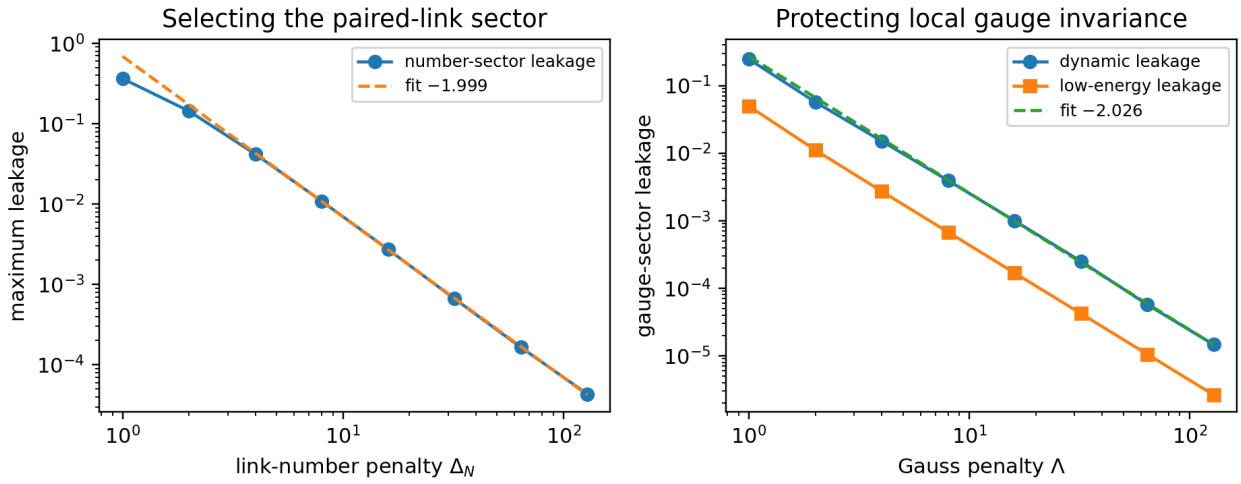

FIG. 4. Low-energy sector selection. (a) A total-number penalty protects the two-ladder spin-S link against generic single-ladder promotions and demotions. (b) A Gauss penalty suppresses both dynamical and low-energy gauge leakage on a four-link plaquette. The measured probabilities follow the expected inverse-square laws.

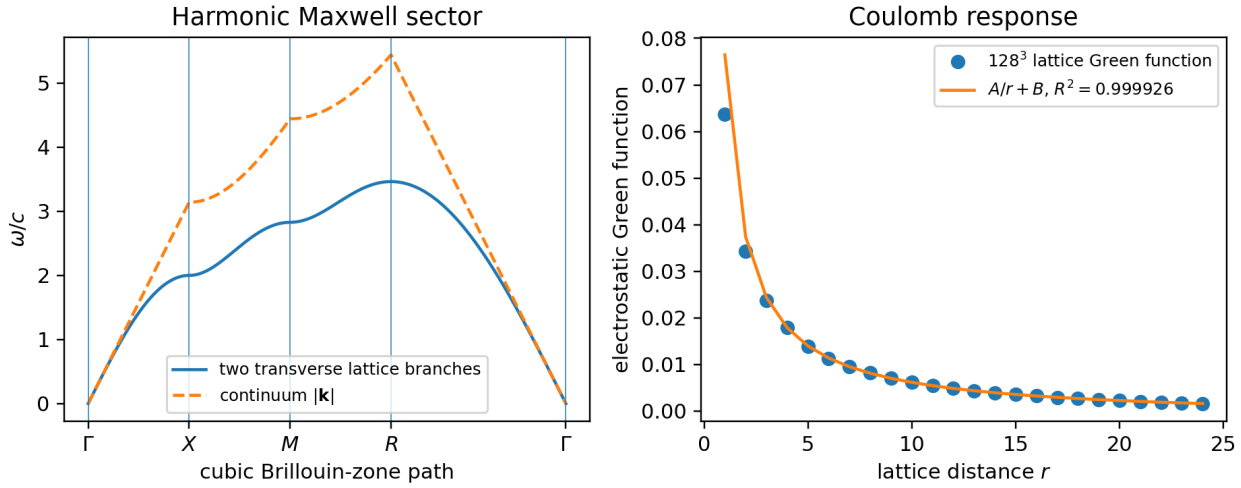

FIG. 5. Maxwell diagnostics of the controlled harmonic sector. (a) The cubic magnetic matrix has two exactly degenerate transverse branches and one longitudinal Gauss redundancy. (b) The periodic lattice Green function follows $A/r + B$ over the scale window between the lattice spacing and system size.

The link-number protection test used two local ladders of dimension eight, $S = 2$, a generic perturbation $0.12(a + a^\dagger + b + b^\dagger)$, and times $0 \le t \le 25$. The Gauss-protection test used an $S = 1$ plaquette, $g^2 = 0.35$, magnetic coefficient $K = 0.55$, gauge-breaking strength 0.18, and $0 \le t \le 30$. The controller gadget used $S = 1$, giving field dimension $3^4 = 81$ and controller-field dimension 324. The Coulomb calculation used FFT inversion of the cubic lattice Laplacian at $L = 32, 48, 64, 96, 128$; the fit coefficient moves monotonically toward the continuum value as L increases.

The accompanying archive contains the complete script, raw JSON, terminal log, figures, and checksums. The script regenerates every number and plot in this article without relying on the autonomous-shutter calculations.

VIII. DISCUSSION: CONSTRUCTION VERSUS INEVITABILITY

The construction establishes a real gauge sector, not a relabeling. The local commutator and gauge transformations are exact at finite dimension; matter hopping and plaquette loops preserve Gauss's law; a microscopic gauge-invariant controller generates the magnetic term; and both the link-number and Gauss sectors can be iso-

TABLE I. Numerical audit of the paired-ladder construction.

check	result
link commutator, $S \leq 64$	4.22×10^{-15}
low-flux unitarity slope	-1.930
one-plaquette gap slope	-1.915
link-number leakage slope	-1.999
Gauss leakage slope	-2.026
gadget Gauss commutator	0
fourth-order ring error	1.82×10^{-16}
Schur-correction slope	2.030
charged-matter commutators	0
Maxwell Ward residual	3.66×10^{-15}
transverse splitting	3.55×10^{-15}
128^3 Coulomb fit	$R^2 = 0.999926$

lated energetically. The large-S low-flux bound then gives a controlled route to the rotor link, whose harmonic three-dimensional sector has the transverse and Coulomb signatures of Maxwell theory.

At the same time, most ingredients have known analogues in quantum-link, bosonic-mapping, gauge-protection, and emergent-$U(1)$ literature [5, 7, 9, 13]. The contribution here is their explicit assembly in the square-root edge-ladder architecture and the quantitative identification of the additional local structures the QATNU substrate requires.

Those additions are substantive. The minimal one-ladder model is replaced by two ladders per oriented link. The total link occupation is selected by Δ_N. Local gauge charge is selected or protected by Λ. Magnetic dynamics requires either an explicit plaquette product or the finite controller gadget of Sec. IV. None follows solely from the statement that an edge register has ladder levels.

The Maxwell calculation is likewise scoped. It proves the harmonic long-wavelength form after the controlled link-to-rotor limit. It does not establish the full compact $3+1$ dimensional phase diagram at every finite small S and coupling, nor derive Lorentz invariance, the observed electromagnetic coupling, or the Standard Model charge spectrum from QATNU parameters. Nonperturbative confirmation of a stable Coulomb phase for a particular finite-S microscopic Hamiltonian would require large-volume simulations of gaps, flux sectors, Wilson loops, and monopole observables.

IX. CONCLUSION

Two square-root edge ladders at fixed total occupation realize an exact finite-dimensional $U(1)$ quantum link. The link's gauge algebra is exact for every S, and its nonunitarity on fixed low-flux states vanishes quadratically with S. Local Gauss generators, gauge-covariant matter hopping, and plaquette loops follow directly. A finite mobile gauge charge generates the magnetic loop at fourth order while preserving the microscopic Gauss law, and energetic penalties suppress violations of both the paired-link and gauge sectors with inverse-square probability laws. The resulting rotor limit has two transverse harmonic modes and a three-dimensional Coulomb response.

The defensible conclusion is therefore precise: a paired-ladder QATNU-compatible extension *supports* a controlled $U(1)$/Maxwell sector. This closes a constructive existence question. It does not prove that the original single-ladder QATNU dynamics inevitably produces electromagnetism or that QATNU is nature's microscopic substrate.

ACKNOWLEDGMENTS

No external funding was used. The numerical audit used NumPy, SciPy, and Matplotlib.

DATA AND CODE AVAILABILITY

The source code, raw JSON output, terminal log, figure-generation script, and SHA-256 checksums are included in the accompanying reproducibility archive. A public archival DOI can be inserted before journal submission.

Appendix A: Proof of the low-flux plaquette bound

On the common interior flux basis, write $U = DV$, where $V|m\rangle = |m+1\rangle$ and $D|m+1\rangle = u_m|m+1\rangle$. Equation (8) gives

$$\|(D - \mathbb{I})V\mathcal{P}_{E_*}\| = \max_{|m|\leq E_*} |1 - u_m| = \delta_S(E_*). \tag{A1}$$

For contractions A_j, B_j, the telescoping identity

$$\prod_{j=1}^{4} A_j - \prod_{j=1}^{4} B_j = \sum_{r=1}^{4} \left(\prod_{j<r} A_j\right)(A_r - B_r)\left(\prod_{j>r} B_j\right) \tag{A2}$$

implies Eq. (10). Applying the same bound to the Hermitian conjugate gives an $8\delta_S$ bound on the magnetic combination $(W + W^\dagger) - (W^{\rm rotor} + W^{\rm rotor\dagger})$ per plaquette, multiplied by its Hamiltonian coefficient.

Appendix B: Gauge invariance of the controller gadget

Let

$$T_x = |x+1\rangle\langle x| \otimes U_x^\dagger. \tag{B1}$$

The controller charge at x decreases by one, the charge at $x+1$ increases by one, and $U_x^\dagger$ lowers the oriented electric

flux by one. Hence the changes cancel independently at both endpoints:

$$[\mathcal{G}_x, T_x] = [\mathcal{G}_{x+1}, T_x] = 0, \tag{B2}$$

while all other generators commute trivially. Since H_0 is diagonal in controller position, Eq. (19) follows. Four clockwise hops produce $W_p^\dagger$ and four counterclockwise hops produce W_p. Three reduced resolvents contribute $(-1/\Delta)^3$, yielding Eq. (20).

Appendix C: Leakage bound

Project the eigenvalue equation $H_\Lambda \psi = E\psi$ onto Q:

$$\left[Q(H_{\text{inv}} + V_b)Q + \Lambda Q \sum_x G_x^2 Q - EQ \right] Q\psi = -QV_bP\psi. \tag{C1}$$

The assumed gap lower-bounds the bracket by the denominator in Eq. (23). Inverting it and taking norms proves the result. The analogous number-sector bound follows after replacing $\sum_x G_x^2$ by $\sum_\ell (N_\ell - 2S)^2$.

[1] K. G. Wilson, Confinement of quarks, Physical Review D **10**, 2445 (1974).

[2] J. Kogut and L. Susskind, Hamiltonian formulation of wilson's lattice gauge theories, Physical Review D **11**, 395 (1975).

[3] J. B. Kogut, An introduction to lattice gauge theory and spin systems, Reviews of Modern Physics **51**, 659 (1979).

[4] D. Horn, Finite matrix models with continuous local gauge invariance, Physics Letters B **100**, 149 (1981).

[5] S. Chandrasekharan and U.-J. Wiese, Quantum link models: A discrete approach to gauge theories, Nuclear Physics B **492**, 455 (1997), arXiv:hep-lat/9609042.

[6] U.-J. Wiese, From quantum link models to d-theory: A resource efficient framework for the quantum simulation and computation of gauge theories, Philosophical Transactions of the Royal Society A **380**, 20210068 (2022), arXiv:2107.09335.

[7] D. Banerjee, M. Dalmonte, M. Müller, E. Rico, P. Stebler, U.-J. Wiese, and P. Zoller, Atomic quantum simulation of dynamical gauge fields coupled to fermionic matter: From string breaking to evolution after a quench, Physical Review Letters **109**, 175302 (2012), arXiv:1205.6366.

[8] A. Mil, T. V. Zache, A. Hegde, A. Xia, R. P. Bhatt, M. K. Oberthaler, P. Hauke, J. Berges, and F. Jendrzejewski, A scalable realization of local u(1) gauge invariance in cold atomic mixtures, Science **367**, 1128 (2020).

[9] J. Osborne, B. Yang, I. P. McCulloch, P. Hauke, and J. C. Halimeh, Spin-s u(1) quantum link models with dynamical matter on a quantum simulator (2023), arXiv:2305.06368.

[10] T. V. Zache, M. Van Damme, J. C. Halimeh, P. Hauke, and D. Banerjee, Toward the continuum limit of a (1+1)-dimensional quantum link schwinger model, Physical Review D **106**, L091502 (2022), arXiv:2104.00025.

[11] M. Hermele, M. P. A. Fisher, and L. Balents, Pyrochlore photons: The u(1) spin liquid in a s=1/2 three-dimensional frustrated magnet, Physical Review B **69**, 064404 (2004), arXiv:cond-mat/0305401.

[12] M. Levin and X.-G. Wen, Quantum ether: Photons and electrons from a rotor model, Physical Review B **73**, 035122 (2006), arXiv:hep-th/0507118.

[13] J. C. Halimeh and P. Hauke, Reliability of lattice gauge theories, Physical Review Letters **125**, 030503 (2020), arXiv:2001.00024.

[14] M. Van Damme, H. Lang, P. Hauke, and J. C. Halimeh, Reliability of lattice gauge theories in the thermodynamic limit, Physical Review B **105**, 245121 (2022), arXiv:2104.07040.